

# Spontaneous emission in Casimir-Rabi oscillations through a weak optomechanical coupling

Ke-Xiong Yan,<sup>1,2</sup> Yuan Qiu,<sup>1,2</sup> Yang Xiao,<sup>1,2</sup> Jie Song,<sup>3</sup> Ye-Hong Chen,<sup>1,2,4,\*</sup> and Yan Xia<sup>1,2,†</sup>

<sup>1</sup>*Fujian Key Laboratory of Quantum Information and Quantum Optics, Fuzhou University, Fuzhou 350116, China*

<sup>2</sup>*Department of Physics, Fuzhou University, Fuzhou 350116, China*

<sup>3</sup>*Department of Physics, Harbin Institute of Technology, Harbin 150001, China*

<sup>4</sup>*Theoretical Quantum Physics Laboratory, Cluster for Pioneering Research, RIKEN, Wako-shi, Saitama 351-0198, Japan*

(Dated: November 7, 2024)

The dynamical Casimir effect (DCE) describes the energy conversion from a mechanical motion to the electromagnetic fields. When the mechanical oscillator is in a mechanically excited state, the free evolution due to the DCE produces radiation in the vacuum, in analogy with the spontaneous emission from an excited atom. In this manuscript, we investigate such a spontaneous radiation process by employing the quantum trajectory approach. When the dissipation rate of the system is very low, there can be a reversible energy exchange between the mirror in the excited state and the vacuum field, and this reversible exchange is called vacuum Casimir-Rabi oscillations. Multiple quantum trajectory simulations of this process show that the number of trajectories responsible for the generation of radiation can reach a significant value when the mechanical dissipation rate is less than the photon dissipation rate. We also find that two-photon (two/three-phonon) bundle emission occurs in photon (phonon) emission. In comparison to pure two-photon and three-phonon free dissipation, the probability of two-photon bundle emission and two-phonon bundle emission are observed to be marginally elevated as a consequence of the presence of the DCE. This pattern may assist in developing a deeper comprehension of the physical characteristics of photon and phonon emission in the DCE.

## I. INTRODUCTION

Quantum field theory predicts that the quantum vacuum is not empty, but teeming with virtual particles [1–8]. By applying certain external perturbations, these vacuum fluctuations can be converted into real particles. Examples include the Schwinger effect [1], Hawking radiation [3], Unruh effect [9], and dynamical Casimir effect (DCE) [6–8, 10, 11]. As one of the most representative examples, the DCE describes the generation of photons due to rapid changes in the geometry (in particular the positions of some boundaries) or material properties of electrically neutral macroscopic or mesoscopic objects. Although DCE was predicted in 1976 [2], radiation induced by vibrating mirrors has not yet been observed. One of the main difficulties is that the speed of vibration of mirrors can hardly approach the speed of light [7, 12].

In order to circumvent these difficulties, a number of alternative proposals have been put forth. These theoretical proposals have suggested that the mechanical motion can be replaced with an effective one [13–17], which may be provided by, for example, modulating the light-matter coupling strength in cavity quantum electrodynamics (QED) systems [18–28], modulating the boundary condition of a superconducting waveguide or resonator [6, 29, 30], and using lasers to rapidly modulate the reflectivity of thin semiconductor films [31, 32]. In particular, two noteworthy experimental confirmations

have been attained through the utilisation of a superconducting quantum interference device [6, 7, 29, 30, 33, 34] and Josephson metamaterials [8] to generate an effective motion, respectively. Notwithstanding these accomplishments, we remain eager to observe the DCE resulting from purely mechanical vibrations of mirrors. This is because the energy conversion of the mechanical motion to the electromagnetic field is a key feature of the DCE predicted in its original proposals [2, 7, 11, 12].

In Ref. [35], Macrì *et al.* have found that vacuum radiation can originate from the free evolution of a pure mechanical excited state, which provides a more fundamental explanation of the DCE. They have shown that a resonant production of photons out from the vacuum can be observed even when the mechanical frequency  $\omega_m$  is lower than the cavity-mode frequency  $\omega_c$  in the cavity-optomechanical system. This regime can mitigate the problem mentioned above (i.e. very fast oscillating mirror).

In this manuscript, following Macrì *et al.* [35], we theoretically derive the effective Hamiltonian, which describes the Casimir-Rabi oscillations between the three-phonon state (the third excited state of the mechanical Fock state) and the two-photon state. Such oscillations can be generated under the condition where the mechanical frequency is lower than the optical frequency. This makes it a particularly promising example for experimental investigation. Then, we investigate such a spontaneous radiation process of mechanically excited states through the stochastic evolution of the system wave function [36–39]. The quantum trajectory approach, i.e. the stochastic evolution of the wave function, can readily describe a

\* yehong.chen@fzu.edu.cn

† xia-208@163.com

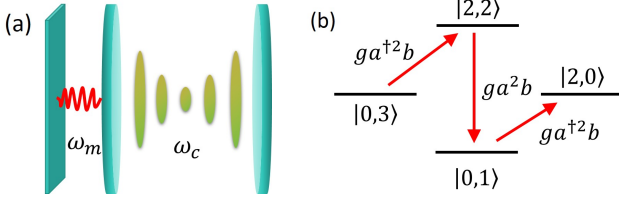


FIG. 1. (a) Schematic of a typical optomechanical system where one of the mirrors in an optical cavity can vibrate at frequency  $\omega_m$ . The resonance frequency of the cavity is  $\omega_c$ . (b) The effective energy level transition process.

single simulation. This allows for the investigation and quantification of the emission of photons and phonons in each DCE simulation.

The rest of the paper is organized as follows: In Sec. II, we introduce the model and calculate the effective Hamiltonian. In Sec. III, the quantum trajectory approach is employed for the investigation of spontaneous radiation from the mechanically excited state. The potential experimental protocols and discussion of parameter sensitivities are presented in Sec. IV and Sec. V, respectively. Finally, the work is summarized in Sec. VI.

## II. THE MODEL AND EFFECTIVE HAMILTONIAN

We consider the case of an optical cavity with a movable end mirror, as schematically depicted in Fig. 1(a). The Hamiltonian of this system can be written as

$$H_s = \omega_c a^\dagger a + \omega_m b^\dagger b + g(a^\dagger + a)^2(b^\dagger + b), \quad (1)$$

where  $a$  ( $a^\dagger$ ) is the annihilation (creation) operator of the optical mode of the cavity with the lowest-frequency  $\omega_c$ . The resonance frequency of the mechanical mode is  $\omega_m$  with bosonic operators  $b$  and  $b^\dagger$ . The optomechanical coupling rate is  $g$ . A detailed derivation of this Hamiltonian can be found in Ref. [40].

By numerically diagonalizing the Hamiltonian  $H_s$  in Eq. (1), we can obtain the energy spectrum of the system. The energy spectrum exhibits numerous avoided crossings [35]. These avoided crossings result from the coherent coupling between the state  $|n, k\rangle$  and the state  $|n+2, k-q\rangle$  with  $k \geq q$ . The variables  $n$ ,  $k$ , and  $q$  denote the number of photon excitations, the number of phonon excitations, and the number of annihilated phonons, respectively. Here, we investigate the coherent coupling between the three-phonon state  $|0, 3\rangle$  and the two-photon state  $|2, 0\rangle$ . The coupling between these two states ensures that the mechanical frequency is lower than the optical frequency, while maintaining a large effective coupling strength. Therefore, we only focus on the fifth excited state and the sixth excited state,

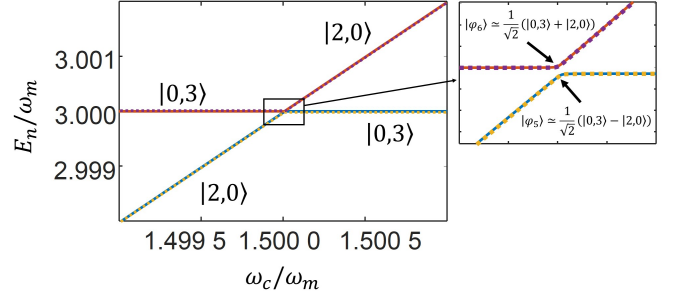


FIG. 2. Eigenvalues  $E_5/\omega_m$  and  $E_6/\omega_m$  as a function of the ratio between the cavity frequency  $\omega_c$  and the mechanical frequency  $\omega_m$ . The continuous curves are the eigenvalues of  $H_s$  in Eq. (1) and the dashed lines describe the eigenenergies of the  $H_{\text{eff}}$  in Eq. (3). Other parameter is  $g = 0.001\omega_m$ .

with the corresponding energy level as a function of the ratio between the cavity and the mechanical frequency presented in Fig. 2. We can see that the two energy levels exhibit an avoided crossing, which serves as a signature of a particular closed subdynamics. When the vacuum Casimir-Rabi splitting [35] is at its minimum (i.e.  $\omega_c \simeq 3\omega_m/2$ ), the two system eigenstates are approximately the symmetric and antisymmetric superposition states

$$|\varphi_{5(6)}\rangle \simeq \frac{1}{\sqrt{2}}(|0, 3\rangle \pm |2, 0\rangle), \quad (2)$$

where  $|n, k\rangle = |n\rangle_c \otimes |k\rangle_m$ .

When the detuning  $\Delta = \omega_c - \omega_m \simeq 1/3\omega_c \gg g$ , an effective Hamiltonian can be derived using the generalized James' effective Hamiltonian method [41] (see Appendix A):

$$\begin{aligned} H_{\text{eff}} &= \omega_c a^\dagger a + \omega_m b^\dagger b + H_{\text{eff}}^{(2)} + H_{\text{eff}}^{(3)}, \\ H_{\text{eff}}^{(2)} &= \frac{g^2}{4\omega_m} [a^\dagger a^2 - 2(2a^\dagger a + 1)(3b^\dagger b + 4a^\dagger a + 3)], \\ H_{\text{eff}}^{(3)} &= \frac{9g^3}{\omega_m^2} (a^\dagger b^3 + a^2 b^\dagger). \end{aligned} \quad (3)$$

The second-order effective Hamiltonian  $H_{\text{eff}}^{(2)}$  leads to a shift in the resonance frequency and the third-order effective Hamiltonian  $H_{\text{eff}}^{(3)}$  is the one responsible for the Casimir-Rabi oscillation between the state  $|0, 3\rangle$  and the state  $|2, 0\rangle$ . In the subspace formed by  $|0, 3\rangle$  and  $|2, 0\rangle$ , the matrix form of the effective Hamiltonian  $H_{\text{eff}}$  can be written as

$$H_{\text{eff}} = \begin{pmatrix} 3\omega_m - \frac{6g^2}{\omega_m} & \frac{18\sqrt{3}g^3}{\omega_m^2} \\ \frac{18\sqrt{3}g^3}{\omega_m^2} & 2\omega_c - \frac{27g^2}{\omega_m} \end{pmatrix}. \quad (4)$$

The aforementioned matrix allows us to ascertain the effective Rabi frequency  $\Omega_{\text{eff}}$  and the resonance condition  $\omega_c$ :

$$\frac{\Omega_{\text{eff}}}{\omega_m} = \frac{18\sqrt{3}g^3}{\omega_m^3}, \quad \frac{\omega_c}{\omega_m} = \frac{3}{2} + \frac{21g^2}{2\omega_m^2}.$$

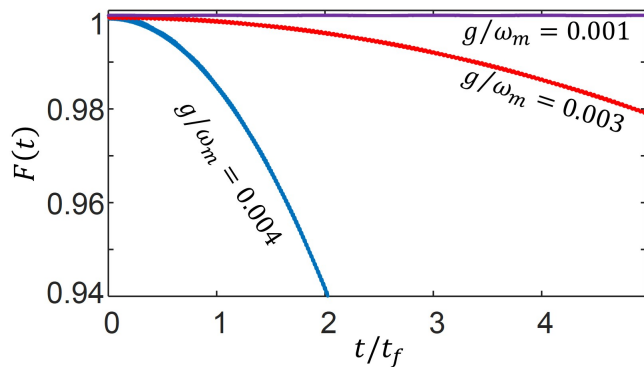


FIG. 3. Fidelity  $F(t)$  defined in Eq. (5) vs the time for various values of the coupling rate:  $g = 0.001\omega_m$  (purple solid curve),  $g = 0.003\omega_m$  (red solid curve), and  $g = 0.004\omega_m$  (blue solid curve). Other parameter are  $\omega_c = 1.5000105\omega_m$  and  $t_f = 1.0077 \times 10^8/\omega_m$ . The initial state of the system is  $|0, 3\rangle$ .

In the derivation of Eq. (3), the rotating-wave approximation (RWA) is employed, necessitating an evaluation of its validity. The validity of the RWA can be ascertained by examining the fidelity

$$F(t) = |\langle \phi(t) | \psi(t) \rangle|^2, \quad (5)$$

between the state  $|\phi(t)\rangle$  obtained by solving the Schrödinger equation with the exact Hamiltonian (1) and the state  $|\psi(t)\rangle$  obtained by solving the Schrödinger equation with the effective Hamiltonian (3). Figure 3 shows that the fidelity undergoes oscillations with time, exhibiting an increase as the coupling strength decreases. When the coupling strength is  $g = 0.001\omega_m$ , the fidelity is observed to stabilize at 1, which provides evidence that the RWA is valid.

### III. SPONTANEOUS EMISSION OF THE MECHANICALLY EXCITED STATE

Spontaneous emission is a process by which a quantum emitter (such as atom and molecule) decays from an excited state to a lower energy state and emits photons [42]. It is a remarkable manifestation of the interaction between a quantum system and vacuum fields. In this section, we discuss the spontaneous emission of the mechanically excited state by following individual trajectories of the evolution of the system.

#### A. quantum trajectory

Dissipation of energy from the system to environment is typically treated by a density operator approach, which is also known as a master equation approach. This approach is capable of describing the ensemble average over numerous trajectories of a quantum system, but requires substantial computational resources [43]. By solving the

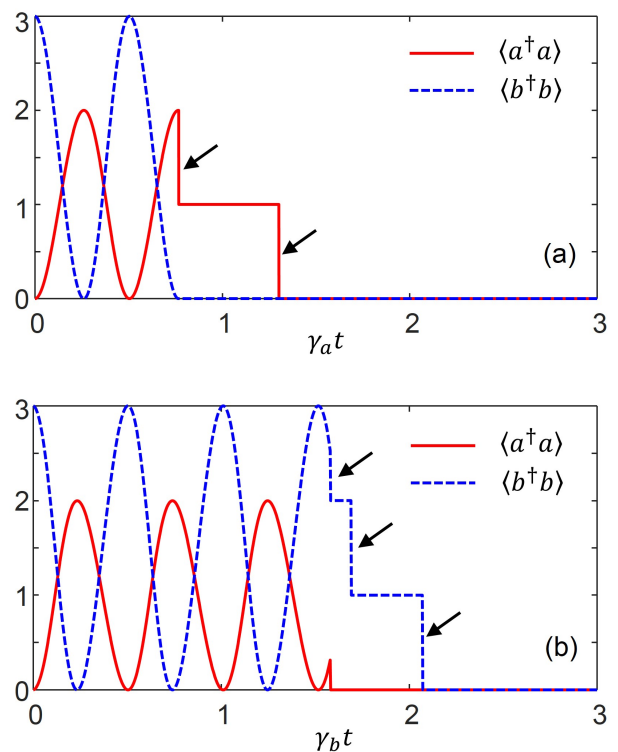


FIG. 4. Examples of a single quantum trajectory, numerically obtained by studying the open quantum dynamics. It shows the time evolution of the mean excitation number of the radiation field  $\langle a^\dagger a \rangle$  (red solid curve) and of the mechanical oscillator  $\langle b^\dagger b \rangle$  (blue dotted curve). The black arrows in both panels indicate that the system has undergone a quantum jump. In panel (a), the system emits two photons outward with an emission interval less than the photon lifetime. In panel (b), the system emits three phonons outward with an emission interval less than the phonon lifetime. In both panels, the system is initialized in  $|0, 3\rangle$  and other parameters are  $g = 0.001\omega_m$ ,  $\omega_c = 1.5000105\omega_m$ , and  $\gamma_a = \gamma_b = 10^{-9}\omega_m$ .

stochastic evolution of the system wave function [43–46], one can follow the individual trajectories of the system and record the clicks of photons (phonons). This evolution is governed by the Schrödinger equation with a non-Hermitian Hamiltonian (see Appendix B)

$$\mathcal{H} = H_s - i(\gamma_a a^\dagger a + \gamma_b b^\dagger b)/2, \quad (6)$$

where  $H_s$  represents the system Hamiltonian in Eq. (1),  $\gamma_a$  and  $\gamma_b$  are the photonic and mechanical loss rates, respectively.

In the subspace spanned by  $|0, 3\rangle, |2, 0\rangle$ , we can have a simple analytical description. If we initialize the system in the state  $|0, 3\rangle$ , the system state at time  $t$ , before a quantum jump takes place, is

$$|\psi(t)\rangle = e^{-\gamma t/2} [\cos(\Omega_{\text{eff}} t) |0, 3\rangle - i \sin(\Omega_{\text{eff}} t) |2, 0\rangle], \quad (7)$$

where we choose  $\gamma = \gamma_a = \gamma_b$ . After the system wave function is normalised, the evolution equations for the

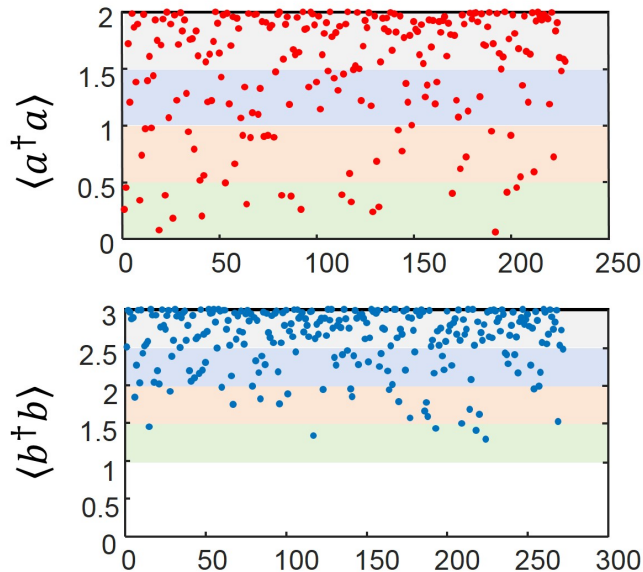


FIG. 5. Statistical plot of the number of photons (phonons) in the system when the first photon (phonon) emission occurs. We run 500 quantum trajectory simulations with 228 trajectories for photon emission and 272 trajectories for phonon emission. All parameters are chosen as in Fig 4.

average phonon number and photon number over time can be obtained:

$$\begin{aligned} \langle a^\dagger a \rangle &= 2 \sin^2(\Omega_{\text{eff}} t) \\ \langle b^\dagger b \rangle &= 3 \cos^2(\Omega_{\text{eff}} t). \end{aligned} \quad (8)$$

The numerical results are shown in Fig. 4. We note that in Fig. 4(a) the system initially oscillates between the state  $|0, 3\rangle$  and the state  $|2, 0\rangle$  predicted by Eq. (8). When a quantum jump occurs, one photon has escaped from the cavity and the state of system collapses to a single photon state  $|1, 0\rangle$ . This state interrupts the Casimir-Rabi oscillation between the state  $|0, 3\rangle$  and the state  $|2, 0\rangle$  and is preserved until a second jump occurs. After the emission of the second photon in the cavity, the system is in the vacuum state  $|0, 0\rangle$ . Throughout the whole process, the system emits only two photons, no phonons are emitted. This is because before the first quantum jump, the system is almost in a two-photon state  $|2, 0\rangle$  with only photon excitation and no phonon excitation. After the quantum jump occurs, the oscillation between the state  $|0, 3\rangle$  and the state  $|2, 0\rangle$  is interrupted, making the conversion between photon and phonon impossible, and there is no more phonon excitation. Similar dynamics process are presented in Fig. 4(b).

The probability of a photon (phonon) jumping in the simulation of quantum trajectories is related to the photon (phonon) excitation number. As illustrated in Fig. 5, a reduction in the number of photon (phonon) excitations is accompanied by a corresponding

decrease in the number of trajectories represented in the colour bar. Among the 272 trajectories of phonon emission, there are 207 trajectories with phonon excitation numbers between 2.5 and 3 at the time of the first phonon emission, while only 77 trajectories have phonon excitation numbers between 2 and 2.5. In the 228 trajectories of photon emission, 149 trajectories exhibit photon excitation numbers ranging from 1.5 to 2 at the time of the first photon emission, whereas only 62 trajectories have photon excitation numbers between 1 and 1.5. This statistical trend indicates that as the number of phonons (or photons) within the system increases, the probability of the system emitting the corresponding particles also increases.

## B. influence of dissipation rate on trajectories

An intriguing physical phenomenon depicted in Fig. 4 warrants further investigation. In the quantum trajectory simulation, the selection of the system's dissipation channel is found to be proportional to the dissipation rate of the corresponding mode. This implies that as the photon (phonon) dissipation rate increases, the number of trajectories that emit photons (phonons) also increases. This is exemplified by the statistical data presented in Fig. 6, which is obtained by the 500 trajectory simulations. When the phonon dissipation rate is five times larger than the photon dissipation rate, the number of photon emissions is markedly smaller than the number of phonon emissions. When the phonon dissipation rate is equal to or less than the photon dissipation rate, the number of photon emissions becomes significant. This indicates that a minimal mechanical dissipation rate is helpful to discern the photons generated by a DCE simulation. A further noteworthy outcome is that the ratio between the number of trajectories for two-photon (two/three phonon) bundle emission and the number of trajectories for photon (phonon) emission exhibits no correlation with the photon (phonon) dissipation rate. Since the time interval between the emission of two photons (two phonons) is less than the photons lifetime  $1/\gamma_a$  (or the phonons lifetime  $1/\gamma_b$ ), such an emission can be considered a bundle emission [45, 47].

For comparisons, we have simulated two- and three-photon emission in the absence of Casimir-Rabi oscillations using the quantum trajectory approach. As illustrated in Fig. 7, the probability of two-photon and two-phonon bundle emission is higher in the presence of Casimir-Rabi oscillations than in its absence. This is due to the fact that Casimir-Rabi oscillations cause the system to oscillate between the two-photon state and the three-phonon state, resulting in fluctuations in the probability of photon and phonon emission. This fluctuation affects the emission interval between two photons or two phonons, thereby increasing the probability of two-photon and two-phonon bundle

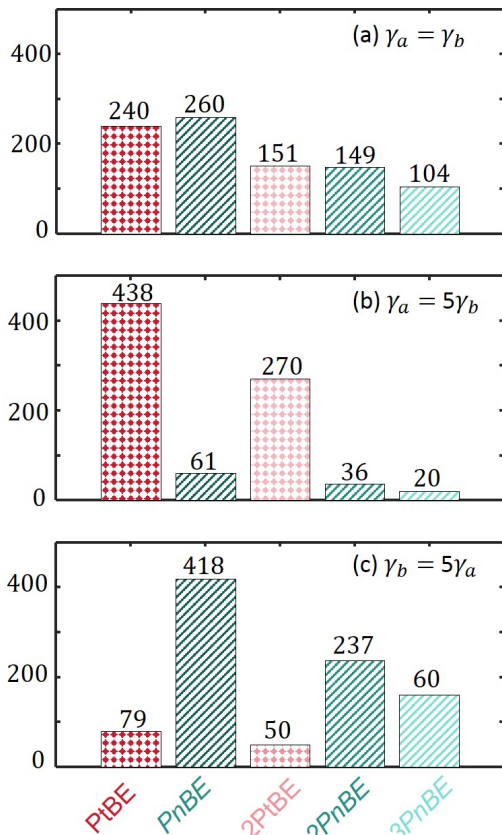


FIG. 6. Statistical results for 500 quantum trajectories. The labels PtBE, PnBE, 2PtBE, 2PnBE, and 3PnBE have been used to denote photon emission, phonon emission, two-photon bundle emission, two-phonon bundle emission and three-phonon bundle emission, respectively. The value on each bar indicates the corresponding number of emission in 500 simulations.

emission.

#### IV. EXPERIMENTAL IMPLEMENTATION

As depicted in Fig. 7, a superconducting quantum interference device (SQUID) loop comprising a mechanical vibrating arm is embedded into a coplanar microwave cavity of length  $d$  and frequency  $\omega_{c1}$ , thereby enabling the effective coupling between the mechanical oscillator and the cavity [25, 48–52]. The SQUID can be modeled as a lumped circuit element at the center  $x = 0$  of the cavity. The mechanical oscillator can be modeled as a harmonic oscillator, with the  $y$  coordinate representing the centre-of-mass displacement, an oscillation frequency of  $\omega_{m1}$ , and a mass of  $m$ . The magnetic flux threading the SQUID loop is given by  $\Phi_{\text{ext}}(y) = \Phi_{\text{ext}}(0) + \lambda B_{\text{osc}} l_{\text{osc}} y$ , where  $\Phi_{\text{ext}}(0) \equiv \Phi_{\text{ext}0}$  is the flux with the mechanical oscillator fixed at  $y = 0$ ,  $B_{\text{osc}}$  is the local magnetic field in the vicinity of the mechanical resonator,  $\lambda$  is a dimensionless geometrical factor that accounts for

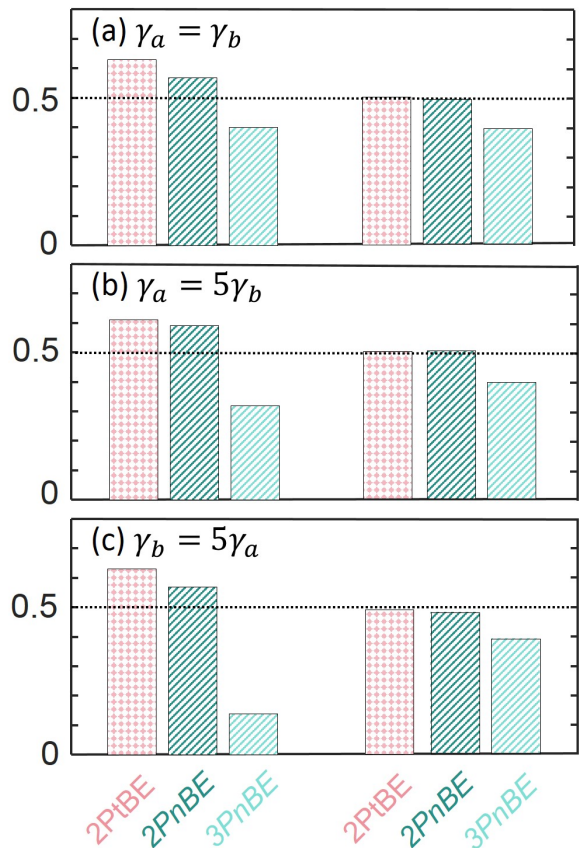


FIG. 7. Histogram of the probabilities for two-photon bundle emission, two-phonon bundle emission and three-phonon bundle emission. The numerical results for the three left columns take into account the interaction of the mirror with the cavity field and the fact that the initial state of the system is a three-phonon state. The numerical results for the three columns on the right do not take into account the interaction of the mirror with the cavity field, and the initial state of the system is a two-phonon state and a three-phonon state, respectively.

the nonuniform displacement of the resonator along its extension. The Hamiltonian, describing the dynamics for the cavity, SQUID, and mechanical oscillator is given by ( $\hbar = 1$ )

$$H_{cSm} = \omega_{c1}^{\text{dc}} a^\dagger a + \omega_{m1} b^\dagger b - \frac{\alpha}{2} (e^{i\omega_{d1}t} + e^{-i\omega_{d1}t}) (a + a^\dagger)^2 - \frac{g_0}{2} (a + a^\dagger)^2 (b + b^\dagger), \quad (9)$$

where the effective cavity frequency is defined to be  $\omega_{c1}^{\text{dc}} \equiv \sqrt{4/C_c d L_J (\Phi_{\text{dc}})}$ . The coupling strengths are expressed as

$$\alpha \equiv \frac{\omega_{c1}^{\text{dc}}}{4} \frac{\pi \delta \Phi}{\Phi_0} \tan \left( \frac{\pi \Phi_{\text{dc}}}{\Phi_0} \right) \quad (10)$$

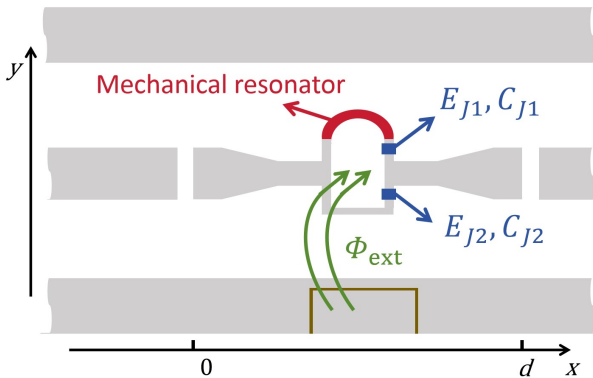


FIG. 8. Layout of a coplanar microwave cavity, characterized by its inductance and capacitance per unit length  $L_c$  and  $C_c$ , respectively, bisected by a dc SQUID. The SQUID is driven by a time-dependent external flux  $\Phi_{\text{ext}}(t)$  (green) and constituted of two Josephson junctions (blue), which are distinguished by their energy  $E_J$ , and capacitance  $C_J$ . One arm of the SQUID loop is mechanically compliant, forming a doubly clamped resonator (red) of length  $l_{\text{res}}$ . For purposes of clarity, the SQUID has been greatly enlarged in this representation with respect to the superconducting cavity.

and

$$g_0 \equiv \omega_{\text{dc}} \frac{\lambda B_{\text{osc}} l_{\text{osc}} y_{\text{zp}}}{\Phi_0 / \pi} \frac{L_J(\Phi_{\text{dc}})}{L_c d} \tan\left(\frac{\pi \Phi_{\text{dc}}}{\Phi_0}\right), \quad (11)$$

where  $\Phi_0 = h/2e$  is the flux quantum and  $y_{\text{zp}} = \sqrt{1/2m\omega_{m1}}$  is the zero-point displacement of the mechanical resonator. Here we suppose that the external flux is weakly modulated around some fixed dc bias  $\Phi_{\text{ext}0} = \Phi_{\text{dc}} + \delta\Phi \cos(\omega_d t)$ . The specific quantisation processes of the circuit in Fig. 7 can be found in Ref. [52]. When the effective cavity frequency and the mechanical oscillation frequency satisfy the resonance condition in Appendix A, we can obtain the same third-order effective Hamiltonian quantity as in Eq. 3.

In the preceding sections, we have assumed that the mechanical oscillator is in an excited state (mechanical Fock state). This state is possible to be prepared, for example, the mechanical oscillator in the SQUID is coupled to an additional qubit [53], using the same protocols realized in circuit QED [54].

## V. PARAMETRIC SENSITIVITY

The resonance between the three-phonon state and the two-photon state is sensitive to the parameters, which can be reflected in the size of the quantum Fisher information (QFI) [55, 56]. Since the system is in a pure state, the QFI relative to the parameter of interest  $A$  can be calculated as [55]

$$\mathcal{F}_A = 4 \left( \langle \partial_A \phi | \partial_A \phi \rangle - |\langle \phi | \partial_A \phi \rangle|^2 \right), \quad (12)$$

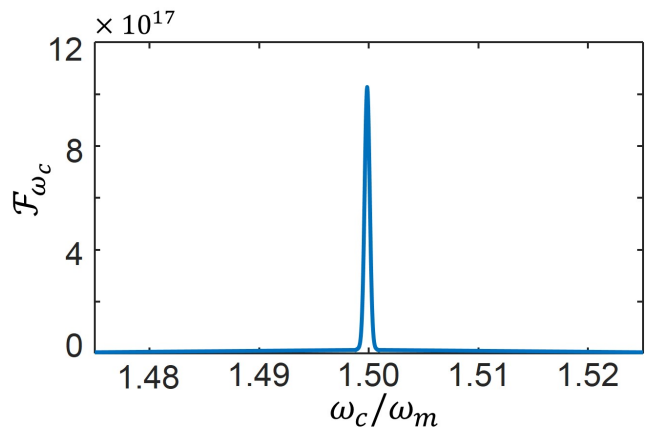


FIG. 9. QFI  $\mathcal{F}_{\omega_c}$  as a function of  $\omega_c$ . For the resonant cavity frequency  $\omega_c = 1.5000105\omega_m$ , QFI has a maximum value. Other parameters are  $g = 0.001\omega_m$  and  $t_f = 1.0077 \times 10^8 / \omega_m$ .

where  $|\phi\rangle$  is the state to be measured. We are interested in the sensitivity of the system evolution to the frequency of the cavity field, so the parameter  $A$  is chosen as  $\omega_c$  and the state

$$|\phi\rangle = \exp^{-i[\omega_c a^\dagger a + \omega_m b^\dagger b + g(a^\dagger + a)^2(b^\dagger + b)]t_f} |0, 3\rangle. \quad (13)$$

In Fig. 9 we can see that QFI is of the order of  $10^{17}$ , which implies that the three-phonon-to-two-photon evolution process is very sensitive to the parameter  $\omega_c$ . This somewhat hinders the experimental observation of photon bundle emission induced by mechanically excited states. Nevertheless, the aforementioned sensitivity offers the potential for precision measurements [55, 57] to be conducted in an experimental setting.

## VI. CONCLUSIONS

We theoretically demonstrate Casimir-Rabi oscillations between three-phonon and two-photon induced by the DCE. By means of the generalized Jame's method, we calculate the effective Hamiltonian of the process. Moreover, we show how the quantum trajectory approach can be employed to investigate spontaneous radiation from mechanically excited states. The outcomes of 500 simulations elucidate the emission patterns of photons and phonons in spontaneous radiation of the DCE. We find that the greater the photon (phonon) dissipation rate, the greater the emission probability of the corresponding particle. The system is most likely to emit photons (phonons) when the photon (phonon) excitation number is at its maximum value. In addition, the presence of Casimir-Rabi oscillations increases the probability of two-photon/phonon bundle emission. Finally, we propose an experimental configuration that may facilitate the implementation of the scheme and illustrate the high sensitivity of the experiment to the parameters by calculating the Fisher information.

The study contributes to a deeper comprehension of the correlation between mechanically excited states and optical field modes in the DCE.

### ACKNOWLEDGEMENTS

Yan Xia was supported by the National Natural Science Foundation of China under Grant No. 62471143, the Key Program of National Natural Science Foundation

of Fujian Province under Grant No. 2024J02008, and the project from Fuzhou University under Grant No. JG2020001-2. Y.-H.C. was supported by the National Natural Science Foundation of China under Grant No. 12304390.

### Appendix A: the derivation of the effective Hamiltonian

To apply the generalized Jame's effective Hamiltonian method [41] to Eq. (1) in the main text, we first rewrite it in the interaction picture,

$$H_I(t) = g[a^\dagger b^\dagger e^{i(2\omega_c + \omega_m)t} + a^\dagger b e^{i(2\omega_c - \omega_m)t} + (2a^\dagger a + 1)b^\dagger e^{i\omega_m t}] + \text{H.c.} \quad (\text{A1})$$

This can also be written in the following form:

$$H_I(t) = \sum_{k=1}^3 [h_k e^{i\omega_k t} + \text{H.c.}], \quad (\text{A2})$$

where

$$\begin{aligned} h_1 &= ga^\dagger b, & \omega_2 &= 2\omega_c - \omega_m, \\ h_2 &= ga^\dagger b^\dagger, & \omega_1 &= 2\omega_c + \omega_m, \\ h_3 &= g(2a^\dagger a + 1)b^\dagger, & \omega_3 &= \omega_m. \end{aligned} \quad (\text{A3})$$

In case of all the frequencies  $\omega_k$  being distinct, the second-order and the third-order effective Hamiltonian can be obtained by calculating the following formulas:

$$H_{\text{eff}}^{(2)} = \sum_k \frac{1}{\omega_k} [h_k, h_k^\dagger], \quad (\text{A4})$$

$$\begin{aligned} H_{\text{eff}}^{(3)} &= \sum_{l,k,n} \left\{ \frac{1}{\omega_n(\omega_n - \omega_k)} [h_l h_k^\dagger h_n e^{i(\omega_l - \omega_k + \omega_n)t} + h_l h_k h_n^\dagger e^{i(\omega_l + \omega_k - \omega_n)t} + \text{H.c.}] \right. \\ &\quad \left. + \frac{1}{\omega_n(\omega_n + \omega_k)} [h_l^\dagger h_k h_n e^{i(-\omega_l + \omega_k + \omega_n)t} + \text{H.c.}] \right\}. \end{aligned} \quad (\text{A5})$$

Considering the resonant condition  $2\omega_c = 3\omega_m$ , all frequency contributions which are different from zero can be neglected by performing the rotating-wave approximation, so we have

$$H_{\text{eff}}^{(2)} = \frac{1}{\omega_1} [h_1, h_1^\dagger] + \frac{1}{\omega_2} [h_2, h_2^\dagger] + \frac{1}{\omega_3} [h_3, h_3^\dagger], \quad (\text{A6})$$

$$\begin{aligned} H_{\text{eff}}^{(3)} &= \frac{1}{\omega_1(\omega_1 - \omega_2)} [h_1 h_2^\dagger h_1 + h_1^\dagger h_2 h_1^\dagger] + \frac{1}{\omega_2(\omega_2 - \omega_1)} [h_1 h_1 h_2^\dagger + h_1^\dagger h_1^\dagger h_2] + \frac{1}{\omega_1(\omega_1 + \omega_1)} [h_2^\dagger h_1 h_1 + h_2 h_1^\dagger h_1^\dagger] \\ &\quad + \frac{1}{\omega_3(\omega_3 - \omega_1)} [h_3 h_1^\dagger h_3 + h_3^\dagger h_1 h_3^\dagger] + \frac{1}{\omega_1(\omega_1 - \omega_3)} [h_3 h_3 h_1^\dagger + h_3^\dagger h_3^\dagger h_1] + \frac{1}{\omega_3(\omega_3 + \omega_3)} [h_1^\dagger h_3 h_3 + h_1 h_3^\dagger h_3^\dagger], \end{aligned} \quad (\text{A7})$$

Finally, we get James' effective Hamiltonian as follow

$$H_{\text{eff}} = \omega_c a^\dagger a + \omega_m b^\dagger b + \frac{g^2}{4\omega_m} [a^\dagger a^2 - 2(2a^\dagger a + 1)(3b^\dagger b + 4a^\dagger a + 3)] + \frac{9g^3}{\omega_m^2} (a^\dagger b^3 + a^2 b^\dagger^3) \quad (\text{A8})$$

### Appendix B: Monte Carlo approach to wave function evolution

The Monte Carlo (MC) or quantum jump approach [43–46] allows the simulation of an individual

trajectory of system dynamics. For describing the effect

of the environment (information gained about the state of the system via the environmental measurements), we introduce the non-Hermitian effective Hamiltonian

$$\mathcal{H} = H_s - \frac{i}{2} \sum_m \gamma_m C_m^\dagger C_m. \quad (\text{B1})$$

Here,  $H_s$  represents the system Hamiltonian part of the dynamics, while  $C_m$  are the jump operators, each corresponding to a separate irreversible process with dissipation rate  $\gamma_m$ .

The algorithm to simulate a single trajectory reads as follows:

(i) At the initial time  $t$ , the system is in a normalized state  $|\psi(t)\rangle$ .

(ia) A random number, designated as  $r_1$ , is selected at random between 0 and 1 in order to ascertain whether a quantum jump has occurred.

(ib) A random number, designated as  $r_2$ , is selected at random between 0 and 1 in order to determine which jump operator is to be employed.

(iii) The probability that a quantum jump occurs in a small time  $dt$  is given by

$$\delta p = \sum_m dt \gamma_m \langle \psi(t) | C_m^\dagger C_m | \psi(t) \rangle \quad (\text{B2})$$

such that  $\delta p \ll 1$ .

(iv) If  $\delta p < r_1$ , no quantum jump occurs, and the system evolves as

$$|\psi(t + dt)\rangle = \exp(-i\mathcal{H}dt) |\psi(t)\rangle. \quad (\text{B3})$$

(v) Otherwise, if  $\delta p > r_1$ , a quantum jump occurs. The probability of jump due to the  $m$ th-operator  $C_m$  is given by

$$P_m = [dt \gamma_m \langle \psi(t) | C_m^\dagger C_m | \psi(t) \rangle] / \delta p. \quad (\text{B4})$$

If  $P_m > r_2$ , the state of the system becomes

$$|\psi(t + dt)\rangle = C_m |\psi(t)\rangle. \quad (\text{B5})$$

(vi) Finally, the state  $|\psi(t + dt)\rangle$  is renormalized and used for the next step of the time evolution.

- 
- [1] J. Schwinger, On gauge invariance and vacuum polarization, *Phys. Rev.* **82**, 664 (1951).
- [2] G. T. Moore, Quantum theory of the electromagnetic field in a variable-length one-dimensional cavity, *J. Math. Phys.* **11**, 2679–2691 (1970).
- [3] S. W. Hawking, Black hole explosions?, *Nature* **248**, 30–31 (1974).
- [4] E. Yablonovitch, Accelerating reference frame for electromagnetic waves in a rapidly growing plasma: Unruh-Davies-Fulling-DeWitt radiation and the nonadiabatic Casimir effect, *Phys. Rev. Lett.* **62**, 1742 (1989).
- [5] J. Schwinger, Casimir light: the source., *Proc. Natl. Acad. Sci.* **90**, 2105–2106 (1993).
- [6] C. M. Wilson, G. Johansson, A. Pourkabirian, M. Simoen, J. R. Johansson, T. Duty, F. Nori, and P. Delsing, Observation of the dynamical Casimir effect in a superconducting circuit, *Nature* **479**, 376–379 (2011).
- [7] P. D. Nation, J. R. Johansson, M. P. Blencowe, and F. Nori, Colloquium: Stimulating uncertainty: Amplifying the quantum vacuum with superconducting circuits, *Rev. Mod. Phys.* **84**, 1 (2012).
- [8] P. Lähteenmäki, G. S. Paraoanu, J. Hassel, and P. J. Hakonen, Dynamical Casimir effect in a Josephson metamaterial, *Proc. Natl. Acad. Sci.* **110**, 4234–4238 (2013).
- [9] W. G. Unruh, Notes on black-hole evaporation, *Phys. Rev. D* **14**, 870 (1976).
- [10] G. Barton and C. Eberlein, On quantum radiation from a moving body with finite refractive index, *Ann. Phys.* **227**, 222–274 (1993).
- [11] S. A. Fulling and P. C. W. Davies, Radiation from a moving mirror in two dimensional space-time: conformal anomaly, *Proc. R. Soc. Lond. A* **348**, 393–414 (1976).
- [12] V. V. Dodonov, Current status of the dynamical Casimir effect, *Phys. Scr.* **82**, 038105 (2010).
- [13] M. Uhlmann, G. Plunien, R. Schützhold, and G. Soff, Resonant cavity photon creation via the dynamical Casimir effect, *Phys. Rev. Lett.* **93**, 193601 (2004).
- [14] E. Segev, B. Abdo, O. Shtempluck, E. Buks, and B. Yurke, Prospects of employing superconducting stripline resonators for studying the dynamical Casimir effect experimentally, *Phys. Lett. A* **370**, 202 (2007).
- [15] R. Stassi, A. Ridolfo, O. Di Stefano, M. J. Hartmann, and S. Savasta, Spontaneous conversion from virtual to real photons in the ultrastrong-coupling regime, *Phys. Rev. Lett.* **110**, 243601 (2013).
- [16] Y.-H. Chen, Y. Qiu, A. Miranowicz, N. Lambert, W. Qin, R. Stassi, Y. Xia, S.-B. Zheng, and F. Nori, Sudden change of the photon output field marks phase transitions in the quantum Rabi model, *Commun. Phys.* **7** (2024).
- [17] K.-X. Yan, Y. Qiu, Y. Xiao, Y.-H. Chen, and Y. Xia, Generating three-photon Rabi oscillations without a large-detuning condition, *Phys. Rev. A* **110**, 043711 (2024).
- [18] C. Ciuti, G. Bastard, and I. Carusotto, Quantum vacuum properties of the intersubband cavity polariton field, *Phys. Rev. B* **72**, 115303 (2005).
- [19] S. D. Liberato, C. Ciuti, and I. Carusotto, Quantum vacuum radiation spectra from a semiconductor microcavity with a time-modulated vacuum Rabi frequency, *Phys. Rev. Lett.* **98**, 103602 (2007).
- [20] S. De Liberato, D. Gerace, I. Carusotto, and C. Ciuti, Extracavity quantum vacuum radiation from a single qubit, *Phys. Rev. A* **80**, 053810 (2009).



- [21] D. Hagenmüller, All-optical dynamical Casimir effect in a three-dimensional terahertz photonic band gap, *Phys. Rev. B* **93**, 235309 (2016).
- [22] K. Baker, E. Waks, and T. Hogg, An experimental demonstration of the quantum state discrimination problem, *Nat. Commun.* **8**, 1504 (2017).
- [23] Y.-H. Chen, W. Qin, X. Wang, A. Miranowicz, and F. Nori, Shortcuts to adiabaticity for the quantum Rabi model: Efficient generation of giant entangled cat states via parametric amplification, *Phys. Rev. Lett.* **126**, 023602 (2021).
- [24] M. Cirio, K. Debnath, N. Lambert, and F. Nori, Amplified optomechanical transduction of virtual radiation pressure, *Phys. Rev. Lett.* **119**, 053601 (2017).
- [25] P. Forn-Díaz, L. Lamata, E. Rico, J. Kono, and E. Solano, Ultrastrong coupling regimes of light-matter interaction, *Rev. Mod. Phys.* **91**, 025005 (2019).
- [26] R.-H. Zheng, W. Ning, Y.-H. Chen, J.-H. Lü, L.-T. Shen, K. Xu, Y.-R. Zhang, D. Xu, H. Li, Y. Xia, F. Wu, Z.-B. Yang, A. Miranowicz, N. Lambert, D. Zheng, H. Fan, F. Nori, and S.-B. Zheng, Observation of a superradiant phase transition with emergent cat states, *Phys. Rev. Lett.* **131**, 113601 (2023).
- [27] Y.-H. Chen, Z.-C. Shi, F. Nori, and Y. Xia, Error-tolerant amplification and simulation of the ultrastrong-coupling quantum Rabi model, *Phys. Rev. Lett.* **133**, 033603 (2024).
- [28] W. Qin, A. F. Kockum, C. S. Muñoz, A. Miranowicz, and F. Nori, Quantum amplification and simulation of strong and ultrastrong coupling of light and matter, *Phys. Rep.* **1078**, 1 (2024).
- [29] J. R. Johansson, G. Johansson, C. M. Wilson, and F. Nori, Dynamical Casimir effect in a superconducting coplanar waveguide, *Phys. Rev. Lett.* **103**, 147003 (2009).
- [30] J. R. Johansson, G. Johansson, C. M. Wilson, and F. Nori, Dynamical Casimir effect in superconducting microwave circuits, *Phys. Rev. A* **82**, 052509 (2010).
- [31] M. Crocce, D. A. R. Dalvit, F. C. Lombardo, and F. D. Mazzitelli, Model for resonant photon creation in a cavity with time-dependent conductivity, *Phys. Rev. A* **70**, 033811 (2004).
- [32] Y. Zhang and Z. Zhang, Critical behavior of the 2d Ising model: A Monte Carlo study, *EPL* **72**, 8 (2005).
- [33] D. A. R. Dalvit, Shaking photons out of the vacuum, *Nature* **479**, 303–304 (2011).
- [34] J. R. Johansson, G. Johansson, C. M. Wilson, P. Delsing, and F. Nori, Nonclassical microwave radiation from the dynamical Casimir effect, *Phys. Rev. A* **87**, 043804 (2013).
- [35] V. Macrì, A. Ridolfo, O. Di Stefano, A. F. Kockum, F. Nori, and S. Savasta, Nonperturbative dynamical Casimir effect in optomechanical systems: Vacuum Casimir-Rabi splittings, *Phys. Rev. X* **8**, 011031 (2018).
- [36] N. Gisin, Quantum measurements and stochastic processes, *Phys. Rev. Lett.* **52**, 1657 (1984).
- [37] L. Diósi, Stochastic pure state representation for open quantum systems, *Phys. Lett. A* **114**, 451–454 (1986).
- [38] C. W. Gardiner, A. S. Parkins, and P. Zoller, Wavefunction quantum stochastic differential equations and quantum-jump simulation methods, *Phys. Rev. A* **46**, 4363 (1992).
- [39] W. Nagourney, J. Sandberg, and H. Dehmelt, Shelved optical electron amplifier: Observation of quantum jumps, *Phys. Rev. Lett.* **56**, 2797 (1986).
- [40] C. K. Law, Interaction between a moving mirror and radiation pressure: A Hamiltonian formulation, *Phys. Rev. A* **51**, 2537 (1995).
- [41] W. Shao, C. Wu, and X.-L. Feng, Generalized James' effective Hamiltonian method, *Phys. Rev. A* **95**, 032124 (2017).
- [42] Y. Yamamoto, S. Machida, and G. Björk, Microcavity semiconductor laser with enhanced spontaneous emission, *Phys. Rev. A* **44**, 657 (1991).
- [43] J. Dalibard, Y. Castin, and K. Mølmer, Wave-function approach to dissipative processes in quantum optics, *Phys. Rev. Lett.* **68**, 580 (1992).
- [44] K. Mølmer, Y. Castin, and J. Dalibard, Monte Carlo wave-function method in quantum optics, *J. Opt. Soc. Am. B* **10**, 524 (1993).
- [45] Q. Bin, X.-Y. Lü, F. P. Laussy, F. Nori, and Y. Wu,  $n$ -phonon bundle emission via the Stokes process, *Phys. Rev. Lett.* **124**, 053601 (2020).
- [46] E. Russo, A. Mercurio, F. Mauceri, R. Lo Franco, F. Nori, S. Savasta, and V. Macrì, Optomechanical two-photon hopping, *Phys. Rev. Res.* **5**, 013221 (2023).
- [47] Q. Bin, H. Jing, Y. Wu, F. Nori, and X.-Y. Lü, Nonreciprocal bundle emissions of quantum entangled pairs, *Phys. Rev. Lett.* **133**, 043601 (2024).
- [48] T. Niemczyk, F. Deppe, H. Huebl, E. P. Menzel, F. Hocke, M. J. Schwarz, J. J. Garcia-Ripoll, D. Zueco, T. Hümmer, E. Solano, A. Marx, and R. Gross, Circuit quantum electrodynamics in the ultrastrong-coupling regime, *Nat. Phys.* **6**, 772–776 (2010).
- [49] A. Frisk Kockum, A. Miranowicz, S. De Liberato, S. Savasta, and F. Nori, Ultrastrong coupling between light and matter, *Nat. Rev. Phys.* **1**, 19–40 (2019).
- [50] A. Blais, A. L. Grimsmo, S. M. Girvin, and A. Wallraff, Circuit quantum electrodynamics, *Rev. Mod. Phys.* **93**, 025005 (2021).
- [51] D. Ballester, G. Romero, J. J. García-Ripoll, F. Deppe, and E. Solano, Quantum simulation of the ultrastrong-coupling dynamics in circuit quantum electrodynamics, *Phys. Rev. X* **2**, 021007 (2012).
- [52] P. D. Nation, J. Suh, and M. P. Blencowe, Ultrastrong optomechanics incorporating the dynamical Casimir effect, *Phys. Rev. A* **93**, 022510 (2016).
- [53] A. D. O'Connell, M. Hofheinz, M. Ansmann, R. C. Bialczak, M. Lenander, E. Lucero, M. Neeley, D. Sank, H. Wang, M. Weides, J. Wenner, J. M. Martinis, and A. N. Cleland, Quantum ground state and single-phonon control of a mechanical resonator, *Nature* **464**, 697–703 (2010).
- [54] M. Hofheinz, H. Wang, M. Ansmann, R. C. Bialczak, E. Lucero, M. Neeley, A. D. O'Connell, D. Sank, J. Wenner, J. M. Martinis, and A. N. Cleland, Synthesizing arbitrary quantum states in a superconducting resonator, *Nature* **459**, 546–549 (2009).
- [55] L. Garbe, M. Bina, A. Keller, M. G. A. Paris, and S. Felicetti, Critical quantum metrology with a finite-component quantum phase transition, *Phys. Rev. Lett.* **124**, 120504 (2020).
- [56] J.-H. Lü, W. Ning, X. Zhu, F. Wu, L.-T. Shen, Z.-B. Yang, and S.-B. Zheng, Critical quantum sensing based on the Jaynes-Cummings model with a squeezing drive, *Phys. Rev. A* **106**, 062616 (2022).
- [57] V. Giovannetti, S. Lloyd, and L. Maccone, Quantum metrology, *Phys. Rev. Lett.* **96**, 010401 (2006).